REPORT DOCUMENTATION PAGE

Form Approved
OMB No. 0704-0188

1. REPORT DATE *(DD-MM-YYYY)*	2. REPORT TYPE	3. DATES COVERED *(From - To)*
19-07-2011	Conference Paper	

4. TITLE AND SUBTITLE

Studies in Optimizing the Film Flow Rate for Liquid Film Cooling

5a. CONTRACT NUMBER

5b. GRANT NUMBER

5c. PROGRAM ELEMENT NUMBER

6. AUTHOR(S)
Ryan P. Miller and Edward B. Coy

5d. PROJECT NUMBER

5f. WORK UNIT NUMBER
50260548

7. PERFORMING ORGANIZATION NAME(S) AND ADDRESS(ES)

Air Force Research Laboratory (AFMC)
AFRL/RZSA
10 E. Saturn Blvd.
Edwards AFB CA 93524-7680

8. PERFORMING ORGANIZATION REPORT NUMBER

AFRL-RZ-ED-TP-2011-309

9. SPONSORING / MONITORING AGENCY NAME(S) AND ADDRESS(ES)

Air Force Research Laboratory (AFMC)
AFRL/RZS
5 Pollux Drive
Edwards AFB CA 93524-7048

10. SPONSOR/MONITOR'S ACRONYM(S)

11. SPONSOR/MONITOR'S NUMBER(S)
AFRL-RZ-ED-TP-2011-309

12. DISTRIBUTION / AVAILABILITY STATEMENT

Approved for public release; distribution unlimited (PA #11312).

13. SUPPLEMENTARY NOTES
For presentation at the 47th AIAA Joint Propulsion Conference, San Diego, CA, 31 July-3 Aug 2011.

14. ABSTRACT

In the production of structures made from reinforced cyanate ester resins, nearly complete cyclotrimerization of the resin with concomitant macromolecular network formation must be achieved in order to ensure adequate mechanical performance and durability of the structures. In the course of developing a wide variety of new cyanate ester resins, as well as in studies of co-cured blends, it has become apparent that some resins can be fully cured into robust networks quite readily under benign conditions, even with a very limited degree of catalysis. Others, though, require post-cure at such high temperatures that the resin undergoes thermochemical degradation during the cure process, while still others are unable to achieve a high degree of cure or form a macromolecular network under any known conditions. Because of the highly selective nature of cyanate ester cyclotrimerization, these differences provide an exceptional opportunity to study the influence of the molecular structure of the monomer on the ability to form a fully cured network structure. For dicyanates of the bisphenol type in particular, studies of cure kinetics and network formation employing differential scanning calorimetry, infrared spectroscopy, and thermomechanical analysis have helped to illuminate important aspects of the links among molecular rigidity, molecular topology, thermal activation, and network formation..

15. SUBJECT TERMS

16. SECURITY CLASSIFICATION OF:			17. LIMITATION OF ABSTRACT	18. NUMBER OF PAGES	19a. NAME OF RESPONSIBLE PERSON
					Dr. Edward B. Coy
a. REPORT	b. ABSTRACT	c. THIS PAGE	SAR	21	19b. TELEPHONE NUMBER *(include area code)*
Unclassified	**Unclassified**	**Unclassified**			N/A

Studies in Optimizing the Film Flow Rate for Liquid Film Cooling

Ryan P. Miller[1]
Purdue University, West Lafayette, IN, 47906

and

Edward B. Coy[2]
Air Force Research Laboratory, Edwards AFB, CA, 93524

Liquid film cooling is an important method for cooling the walls of a liquid rocket engine. Mass transfer via entrainment decreases the effectiveness of the film coolant and it is therefore important to estimate the amount of film coolant that establishes itself along the wall of a combustion chamber if the coolant flow rate is to be optimized. However, film entrainment research is limited in regards to film cooling applications in rockets. The correlations and theories that have been published are often contradictory and have only been tested at momentum fluxes that are an order of magnitude less than those typically experienced in rockets. Experimental research has been conducted in a cold-flow test article at AFRL in order to investigate the effects of gas stream momentum flux on the optimal liquid flow rate. This paper summarizes the results of these tests. In addition, the thickness of the liquid film appears to be an important variable governing the establishment of the liquid film. This paper also investigates the ability of laser focus displacement meter (LFD) to measure the thickness of shear-driven liquid films driven by gas-phase momentum fluxes ranging from 2,270 Pa to 110,000 Pa.

Nomenclature

A	=	cross-sectional area of of channel
b	=	film width
EF	=	entrainment fraction
D	=	diameter
f	=	distance from focal point to liquid film surface
Fr	=	Froude number
LFD	=	laser focus displacement meter
M	=	momentum flux
n	=	index of refraction
r	=	radius
Re	=	Reynolds number
s	=	horizontal offset distance
V	=	velocity
We	=	Weber number
T	=	temperature
X_e	=	entrainment parameter

[1] Graduate Student, School of Aeronautics and Astronautics, Member AIAA.
[2] Mechanical Engineer, RZSA, Member AIAA.

Subscripts

1	=	property in gas
2	=	property in liqud film
a	=	air
ave	=	average
D	=	diameter
E	=	Ebner's definition
δ	=	film thickness
f	=	liquid film
g	=	gas phase
h	=	hydraulic
l	=	left
r	=	right
hc	=	half-cone
T	=	Total
S	=	Sawant's definition

Greek Symbols

α	=	surface angle of liquid film
δ	=	film thickness
μ	=	absolute viscosity
σ	=	surface tension
τ	=	shear stress
ρ	=	density
θ	=	angle
Γ	=	liquid film flow rate per unit circumfernce
φ	=	angle of inclination of test article
λ	=	dimensionless film length

Definitions

j = $\dot{V}/A$ = Superficial Velocity

δ^+ = $\frac{\delta}{\nu}\sqrt{\frac{\tau_s}{\rho}}$ = dimensionless film thickness

w^+ = Γ/μ_f = dimensionless injected liquid flow rate

Introduction

Liquid film cooling is an effective means of protecting the wall of a combustion chamber and throat in liquid rocket engines. In addition, it may also serve to protect the wall from potentially damaging reactions with species in the core flow. A limitation associated with liquid film cooling is that it reduces the temperature of the combustion gases, thereby resulting in a performance loss. Therefore, it is undesirable to inject more film cooling than what is needed and it is important to optimize the liquid film flow rate in order to achieve the best possible performance in liquid rockets.

The effectiveness of liquid film cooling has been demonstrated in the recent literature. Volkmann[1] studied the effects of film cooling on reducing the heat flux experienced at the throat of a rocket. Tests were conducted in a subscale LOX/RP-1 2000 psia combustor. Film coolant was injected at 4.4 inches upstream of a nozzle throat and 16.4 inches upstream. The peak heat flux recorded without film cooling was about 65 Btu/in^2-s, whereas the peak heat flux was about 48 Btu/in^2-s with 16.4 inches upstream film injector and 20 Btu/in^2-s with the 4.4 inches upstream injector. Kirchberger[2] conducted film cooling experiments on a 1500 psi bench-scale heat-sink test article

running on GOX and kerosene. His results showed that kerosene is a much more effective film coolant than nitrogen.

Liquid hydrocarbon (LHC) fuel film cooling (FFC) can be decomposed into a number of sub-processes as shown in Fig. 1. When liquid is introduced through a slot into a high velocity, reacting flow, a portion may be stripped from the surface and entrained into the gas stream. This portion may undergo secondary atomization before vaporizing and chemically reacting. The remainder will attach to the wall and form a film layer. The film will be subjected to shear stress and convective and radiative heat flux from the overlying gas flow and as well as boundary conditions of no-slip, temperature and heat flux from the underlying wall. Surface disturbances may be created resulting in additional stripping and entrainment while heat transfer will vaporize the fuel. If the combustion gases are fuel rich, the addition of additional fuel vapor to the overlying boundary layer will reduce the energy of the gas and lower the rate of heat transfer to the film. Vaporization may also produce a "blowing" effect, or Stefan flow, due to the high rate of mass transfer that may further reduce the rate at which hot gas penetrates the liquid film layer. After an initial heat up distance, the film can reach the wet bulb temperature when the loss of energy by vaporization and conduction to the wall is balanced by the rate of heat addition. It is also possible that the fuel layer will transition to a supercritical state at which point surface tension will not exist and the rate of mixing with the overlying gas would increase. In either case, a fuel rich layer will persist for some distance downstream until mixing, decompostion, and oxidation return the gas temperature to the level that existed upstream of the slot. The fuel and fuel rich products may undergo thermal cracking and deposit solid carbonaceous material (coke) on the chamber wall. This layer will insulate the wall of the chamber and the surface temperature exposed to the hot gas will rise. It may be efficacious to place a second slot and then a third and so on. The optimal design of a slot injection system may involve several injection points with slot widths, fuel mass flows and spacing that have been designed to meet specific wall temperature requirements while minimizing the negative impact on engine performance.

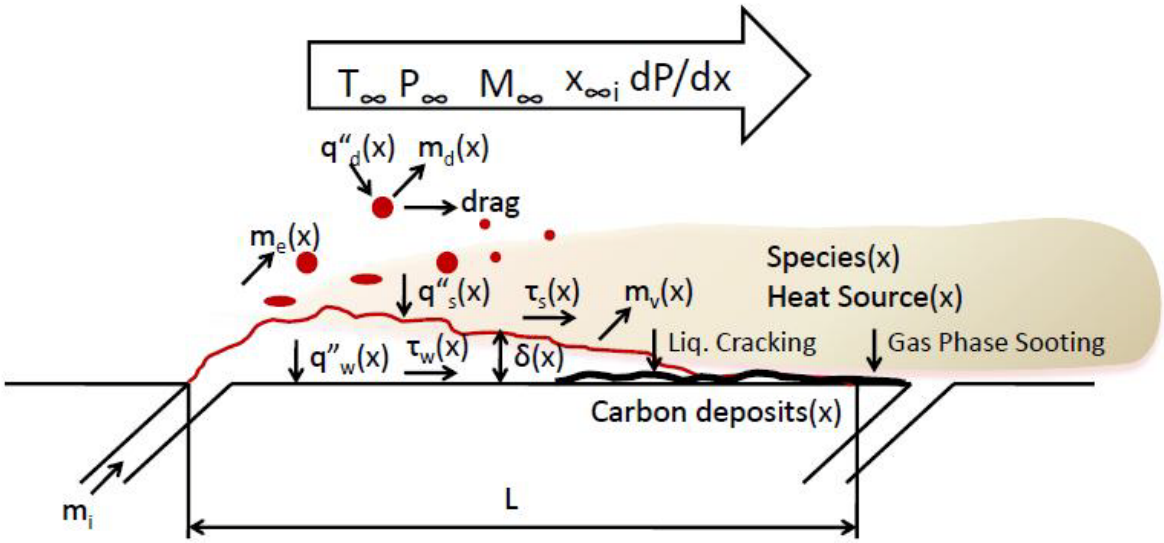

Figure 1: Diagram Illustrating Liquid Film Cooling

In this paper, the establishement of the liquid layer along the wall is examined. Specifically, the effect that the injected liquid flow rate and gas momentum flux have on liquid film entrainment is investigated. To separate the effects of mass transfer due to entrainment from evaporation, the experiments described in this paper have been performed under cold-flow conditions, using nitrogen gas and water as simulants for the combusion gases and film

coolant, respectively. The objective is to determine the optimal liquid flow rate that should be injected through a slot that will optimize cooling effectiveness and reduce performance loss.

Previous studies at AFRL and the literature suggest that the film thickness is an important variable in determining the establishment of the liquid film. Film thicknesses under conditions characteristic of rockets have thus far been difficult to measure as they have been estimated to be on the order of 100 microns or less. In the past decade, research has shown the laser focus displacement (LFD) to be a viable instrument for measuring the thickness of shear-driven liquid films of this scale[3,4]. However, most of the researchers thus far have used the LFD under more benign gas momentum fluxes than those expected in rockets. As a result, the surface of the liquid film was relatively stable under most of the applications for the LFD thus far. Thus, a secondary objective of this paper is to qualify the ability of a Keyence LT-9030 Laser Focus Displacement Meter to measure the thickness of highly turbulent, shear driven liquid films, with gas flows characterized by momentum fluxes upward of 30,000 Pa.

Background of Film Entrainment Studies

The amount of experimental work that has been done to characterize the mechanisms of entrainment and film stability for liquid film cooling applications in rockets is limited.[5] Most of the literature regarding film stability and entrainment for liquid film cooling in rockets occurred prior to 1970. Kinney[6], Knuth[7], and Coy[8] all concluded that the establishment of the liquid film is dominated by a maximum stable liquid film Reynolds number, though the definitions of that Reynolds is different for each researcher. On the other hand, Gater[9] observed that the amount of film entrained into the gas flow is entirely dependent on the momentum flux of the gas phase and surface tension of the film coolant. Ebner[10] conductd experiments on the entrainment fraction of thin oil films at much lower momentum fluxes than the others, but observed that entrainment fraction from a liquid film is dependent on both We_D and Re_D. Finally, Sawant[11] observed that the entrainment fraction in annular flows is primarily dependent on We_D at low We_D and primarily dependent on Re_D at high We_D. In summary, tests that have investigated the phenomena of entrainment from thin liquid films have been limited to momentum fluxes of less than 200,000 Pa, whereas momentum fluxes characteristic of high performance liquid rocket engines are generally above 1,000,000 Pa in the combustion chamber to 10,000,000 Pa at the throat.

Kinney[6] performed extensive experimental heat transfer and cold flow studies on liquid film cooling in the 1950's. Heated air was used to simulate the combustion gases and liquid water was used as the coolant simulant in the heat transfer experiments, while water, aqueous ethylene glycol solutions, and water-detergent solutions were used as coolants to vary surface tension and viscosity in the cold flow experiments. In the heat transfer experiments, it was observed that the film cooling effectiveness began to decrease when the injected non-dimensional coolant flow rate, w^+ (analogous to a liquid film Reynolds number), exceeded about 360. Kinney[6] concluded that this nonlinearity was due to the formation of disturbance waves on the film surface that subsequently lead to droplets being sheared off of the wave crests. It was hypothesized that the surface of the liquid film becomes unstable and waves begin to form once the liquid film is thick enough such that turbulent forces in the gas phase overcome viscous forces in the liquid phase. In their cold-flow experiments, they observed that waves formed on the surface of the liquid film at a w^+ of 90. Kinney[6] concluded that heat transfer to and evaporation from the liquid film had a stabilizing effect, which allowed more coolant to be injected before the effectiveness began to decrease in the heat transfer experiments than what was predicted by the cold-flow experiments. Kinney[6] also observed that the liquid flow rate at which disturbances were first observed increased with increasing viscosity, increased slightly with increased surface tension, and was relatively independent of the gas stream mass velocity.

Later, Knuth[7] extended the results of Kinney's experiments on film stability. Knuth[7] also performed similar cold-flow visualization tests and heat transfer tests to Kinney. Knuth concluded that the maximum stable coolant flow rate, ie. the maximum flow rate before waves are formed, follows the following equation[5,7]:

$$\Gamma_{cr,Knuth} = 1.01 \times 10^5 \left(\frac{\mu_g^2}{\mu_l}\right) \quad (eq.1)$$

Again, both Kinney and Knuth observed that the stable liquid film flow rate seems to be independent of the gas phase momentum flux.

Gater[9] attempted to distinguish the mass transfer by entrainment from the mass transfer by evaporation in his experiments. Gater[9] conducted his experiments with a flat film, as opposed to annular flow, and measured the amount of liquid that remained attached to the wall with a knife-edge capture slot. The film coolants studied were water, methanol, butanol, and RP-1, and the gas was heated air. Contrary to the observations of Kinney and Knuth, Gater[9] observed that the wave structure and instabilities on the surface of the film were dependent only on the momentum flux of the gas stream and surface tension of the liquid film. No dependence on the viscosity of the

liquid film was observed. Secondly, it was observed that the fraction of the liquid film entrained into the gas flow was also only a function of the momentum flux of the gas and surface tension of the liquid film. They proposed the following dimensional, empirical correlation for the entrainment fraction:

$$EF = 1.0 - \exp\left(-5 \times 10^{-5}(X_e - 1000)\right) \quad (eq.2)$$

Where X_e is a dimensional entrainment parameter defined by:

$$X_e = \frac{M_g^{1/2}}{\sigma}\left(\frac{T_g}{T_s}\right)^{1/2} \quad (\mathrm{lb_f})^{-1/2} \quad (\mathrm{eq.}\,3)$$

This correlation is only truly applicable to flat films running through a rectangular duct due to its dimensionality. However, Gater[9] did suggest that X_e could be recast as a Weber number with the wave height on the liquid film taken as the characteristic length.

More recently, Coy[8] estimated the entrainment fraction from a slot injector.. Gas momentum fluxes were 33000 Pa, 66000 Pa, and 99000 Pa and the liquid film was injected at .155, .219, and .268 kg/s-mm. The pressures and temperatures were about ambient and the mach number in the test section was estimated to be about .6. Coy used high speed video to track the disturbance velocity on the liquid film.[7] Assuming couette flow and an empiracal correlation for surface roughness, Coy[8] was able to estimate the thickness of the liquid film. Reducing this thickness to wall coordinates, it was discovered that the δ^+ for all the experimental conditions collapsed to about 20. Coy[8] concluded that a δ^+ of 20 governed the maximum amount of liquid film that could remain attached to the wall before becoming entrained into the gas phase. Any additional liquid injected as a film that would tend to push δ^+ above 20 would become entrained into the gas phase[8].

Ebner[10] researched droplet entrainment from flat, shear-driven oil films at several inclination angles. Ebner performed experiments in an unheated 30 mm X 50 mm rectangular duct. The oil films were injected via a tangential slot and terminated using a knife-edge capture slot at 10, 20, and 30 duct heights away from the injection point. Ebner[10] used a laser focus displacement meter to measure film thickness. The following correlations for film thickness and entrainment fraction were proposed

$$EF = 1.042 \cdot 10^{-7} We_{D,E}^{1.2} Re_{f,E}^{.4} \lambda^{0.8} \left(1 + 2.061 \cdot 10^{-4} \frac{Re_{f,E}^2}{We_{D,E} Fr_f}\right)^{2.25} \quad (eq.4)$$

$$\delta = 1.714 We^{-0.36} Re_f^{0.457} \cdot \left(1 - 1.096 \cdot 10^{-14} \frac{Re_f^4}{Fr_f^2}\right)^{0.375} \quad (eq.5)$$

where:

$$We_{D,E} = \frac{\rho_f u_g^2 D_h}{\sigma} \quad (eq.6)$$

$$Re_{f,E} = \frac{j_f H}{\nu_f} \quad (eq.7)$$

$$Fr_f = \frac{j_f}{Hg \sin\varphi} \quad (eq.8)$$

$$\lambda = \frac{l}{H} \quad (eq.9)$$

Sawant[11] investigated the entrainment fraction in co-current vertical air-water and Freon-113 annular flows. The experiments were conducted for We_D from 0-25000 and for Re_f ranging from 150-5000. Sawant[11] suggested two correlations to estimate the entrainment fraction in vertical upward annular flows for diameters up to 32.0 mm. The simpler of the two (a good approximation of the other) is:

$$EF = \left(1 - \frac{13N_{\mu f}^{-.5} + .3\left(Re_{f,S} - 13N_{\mu f}^{-.5}\right)^{.95}}{Re_{f,S}}\right) \times \tanh\left(2.31 \times 10^{-4} Re_{f,S}^{-.35} We_{D,S}^{1.25}\right) \quad (eq.10)$$

where:

$$N_{\mu} = \frac{\mu_f}{\left(\rho_f \sigma \sqrt{\frac{\sigma}{g\Delta\rho}}\right)^{1/2}} \quad (eq.11)$$

$$Re_{f,S} = \frac{\rho_f j_f D}{\mu_f} \quad (eq.12)$$

$$We_{D,S} = \frac{\rho_g j_g^2 D_h}{\sigma}\left(\frac{\Delta\rho}{\rho_g}\right)^{1/4} \quad (eq.13)$$

This correlation is illustrated in figure 1 for $N_{\mu f}$ = .00266:

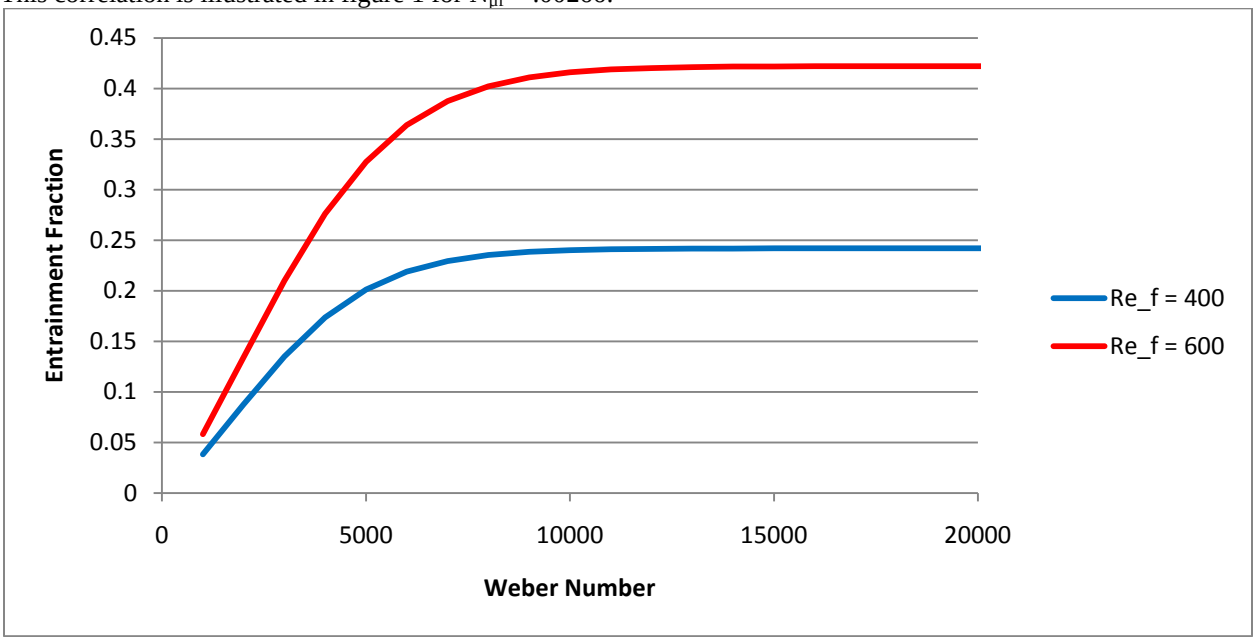

Figure 1: Illustration of of equation 10.

Figure 1 shows that the entrainment fraction in annular pipe flows is mostly dependent on We_D at low We_D and then becomes virtually independent of We_D at increasing values of We_D. Sawant[11] suggested that the change in behavior was due to small entrained droplets decreasing the turbulence intensity in the gas phase, which laminarized the flow above the liquid film, thus shielding the film from the gas. Note that this equation is only valid for fully developed, annular pipe flows of pipe diameters less than 1 inch. Sawant[11] obtained all of his entrainment fraction data at 400 pipe diameters downstream of where the film was injected in his experiments. Thus, equation 6 is not valid for the geometry and conditions of our experiment. However, it is presented here to illustrate expected trends of the dependence of entrainment fraction on some of the two-phase flow variables.

Background on the Use of a Laser Focus Displacement Meter for Measuring Film Thickness

In this experiment, the thickness of the liquid film coolant was chosen to be measured by a Keyence LT-9030 Laser Focus Displacement meter (LFD). This instrument is intended for product testing and quality control whenever small dimensions or thicknesses are important. Common applications for the LFD are measuring the thickness of a contact lens, detecting surface scratches, or measuring surface profiles.

The laser focus displacement meter uses a converging laser beam with an oscillating focal point to detect the location of a surface. When the focal point of the beam is located directly on a surface, the amount of light reflected back to the instrument is at a maximum. Thus, the position of a surface can be determined by correlating peaks in the light intensity being reflected back to the LFD with the position of the focal point. Multiple sufaces can be detected with the LFD, provided that they fall within the range of the focal point's oscillations. For example, if a transparent film falls within the range of the focal point, then both surfaces of the film would be detected, as each surface would reflect its own light intensity peak back to the LFD. A schematic of the operating principle of the LFD is shown in figure 2.

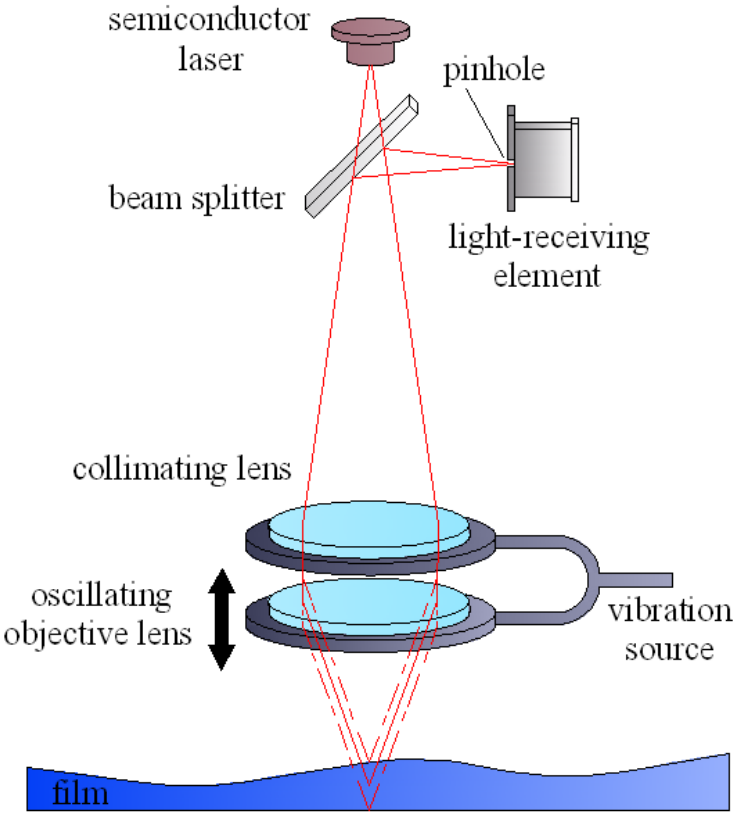

Figure 2: Diagram of LFD operation. Figure taken from Wegener.[3]

While the LFD was not intended to be used to measure the surface of thin wavy, shear-driven films, the LFD has been qualified and used to measure the thickness of liquid films in several experiments.[3,4,10] Wegener[3] evaluated the surface angle limitations of the LFD and demonstrated that the LFD is unable to detect the surface of a liquid film if the suface angle exceeds 8 degrees. Additionally, the frequency response of the LFD (about 550 Hz) is too slow to obtain time-resolved surface profiles of shear-driven liquid films for most applications.[3,10] Despite these limitations, it was concluded that the LFD was capable of giving time-averaged film thicknesses for the experimental conditions studied thus far (generally much lower gas velocities then the ones in our experiment).

The LFD can be set up to measure liquid film thickness in one of two configurations, as shown in figure 3. Thus far, most techniques measured the liquid film thickness by orientating the LFD such that the laser beam passed behind the substrate upon which a liquid film ran, as shown in left-hand side of figure 3. The other technique is to orient the LFD such that the laser passes through the liquid film before contacting the substrate. The advantage with the former techinque is that it avoids entrained droplets from interfering with the laser beam. However, Hazuku[4] observed that this limits the minimum film thickness that the LFD can detect. The minimum detectable film thickness depends on wall inclination angle and surface roughness[4]. Hazuku[4] was unable to detect film thicknesses less than 20-50 µm for this configuratio. It is expected that the liquid films ecountered in our experiment may be on the same order as or smaller than this.[8] Therefore, the latter orientation was chosen for measuring film thickness with the LFD. Note that this is the first time that an attempt has been made to measure the thickness of a shear-driven liquid film using the latter configuration in a high momentum flux, high entrainment environment.

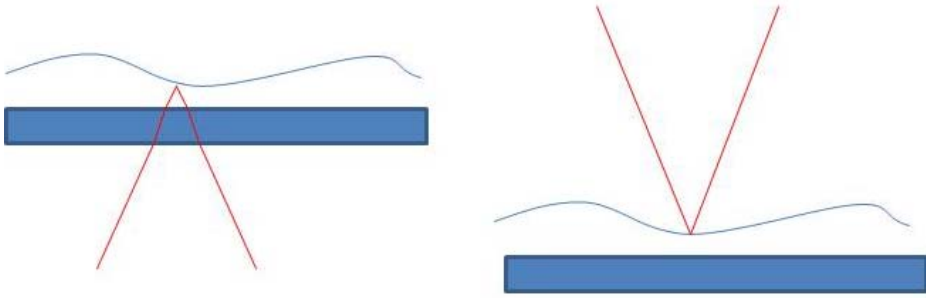

Figure 3: Different Configurations for measuring film thickness

Objectives and scope of current study

As explained previously, studies available in the literature have thus far presented contradictory observations regarding the entrainment and stability of shear driven liquid films. The contradictions in the different researchers' observations can perhaps be explained by examining the experimental conditions of each study. The literature and experiments at AFRL have indicated that the momentum flux of the core gases in a rocket is a dominant variable affecting liquid film stability, entrainment, and overall film cooling effectiveness. Table 1 shows a comparison of the observations and gas momentum fluxes of the experiments described in references 6-11. Upon examination of Figure 1 and Table 1, it is suggested that gas momentum flux and liquid film surface tension are the dominant flow properties governing the establishment of the liquid film when momentum fluxes are low. It appears as though liquid flow rate and coolant viscosity dominate entrainment and liquid film stability at higher momentum fluxes, suggesting a dependence on a liquid film Reynolds number.

Table 1 also shows that the momentum fluxes in all the experiments thus far are about an order of magnitude less than the conditions in liquid rockets. Efforts are currently under way at AFRL to study the establishment of the liquid films in the presence of gas flows with momentum fluxes up to and exceeding 1,000,000 Pa. The experiment described in this paper was intended to study the entrainment fraction for momentum fluxes from 38,000-110,000 Pa and qualify the LFD's ability to measure film thickness under these conditions. The results of the current study will be used to design a new test article capable of higher momentum fluxes. The eventual goal of the research at AFRL is to determine a correlation or criterion that accurately predicts the optimum liquid flow rate to be injected through a slot for the purposes of film cooling.

Researcher	Gas Momentum Flux (Pa)	General Observations
Kinney[6]	40,000 - 200,000	Cooling Effectiveness dependent on coolant viscosity and coolant flow rate. Little dependence on gas momentum flux and surface tension
Knuth[7]	40,000 - 200,000	Cooling Effectiveness dependent on coolant viscosity and coolant flow rate. Little dependence on gas momentum flux and surface tension
Gater[9]	1000 - 30000, with one case at 54,000	Entrainment fraction dependent on gas momentum flux and surface tension. Little dependence on coolant viscosity and coolant flow rate
Coy[8]	33,000 - 99,000	Maximum amount of coolant that remained attached to the wall seemed to be governed by $\delta^+ = 20$
Ebner[10]	850 - 4,500	Entrainment fraction dependent on both a We_D and $Re_{f,D}$
Sawant[11]	1000-200,000	Entrainment fraction dependent on both a We_D and $Re_{f,D}$
Current Experiment	38,000 - 110,000	
Proposed Experiment	10,000 – 1,000,000	
High Pressure Liquid Rockets (combustion chamber)	>1,000,000	
High Pressure Liquid Rockets (throat)	approx. 10,000,000	

Table 1: Comparison of the Momentum Flux of Several Experiments.

Description of Experiment, Results, and Discussion

Cold flow tests with nitrogen and water were conducted at AFRL in order to better understand the entrainment from shear-driven liquid films. A schematic of the test article is shown in figure 4. For each test, gaseous nitrogen was metered with a sonic nozzle and water flow was metered with a cavitating venturi. The static pressure of the test section was monitored via the pressure tap located 1 inch upstream of the slot. Two differential pressure taps were located at 25.4 mm and 127 mm downstream of the injection slot in order to estimate the additional pressure drop and shear stress asscociated with the liquid film. The Mach number in the test section was controlled by inserting cylindrical plugs of various diameters at the exit of the test section. The liquid film was removed at 139.7 mm downstream of the injection slot via a film removal slot. The liquid and some of the entrained gas that was removed through the slot was then passed to a gas/liquid separator. For each test run, the liquid flow rate that was removed via the gas liquid separator was measured by collecting the liquid in a beaker and measuring the time to fill with a stop watch. The top of the film removal slot was between 0 and 25 microns above the film panel and was about .76 mm in the streamwise direction.

Figure 4 shows an image taken from the high speed video camera during a typical test run. It appears as though the liquid is issuing uniformly from the injection slot. The film appears to be slightly pulling away from the right wall in the figure due to surface tension affects. A shadow is currently obstructing a better view of the left side of the test section in this image. However, visual inspection during the experiments showed that liquid film was attached to the left wall.

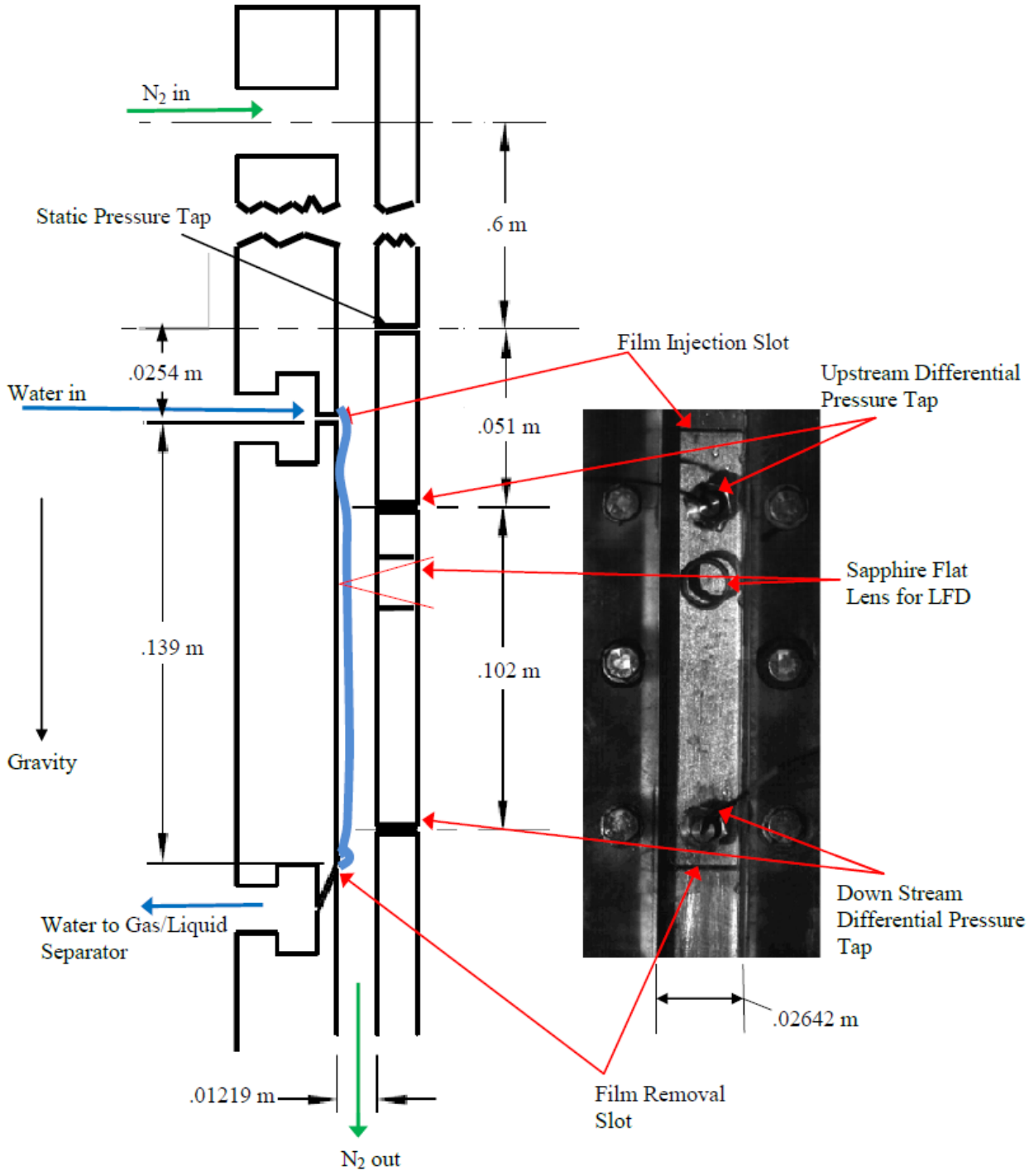

Figure 4: Diagram of Test Article (Left) and a High Speed Video Image During a Test Run (Right)

The primary function of the the high speed video in these experiments was to verify the effectiveness of the removal slot. In figure 4, it appears as though the removal slot is effective in removing all of the liquid film. However, figure 5 shows images taken before and after the valve running the removal slot was opened at a much higher resolution than the image in figure 4. In figure 5, it appears that a small amount of film is escaping over the

removal slot. The images of the removal slot appeared to be almost identical for all test conditions. Therefore, the removal slot was not completely effective in removing the film during any of the experiments.

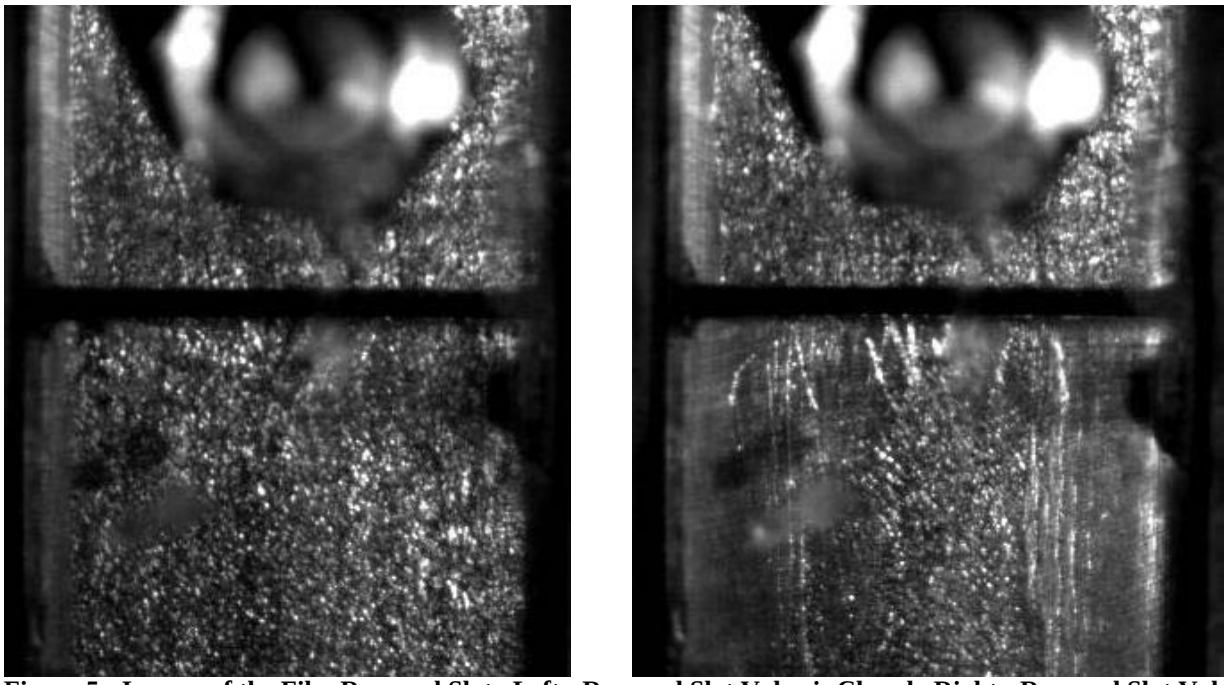

Figure 5: Images of the Film Removal Slot. Left: Removal Slot Valve is Closed. Right: Removal Slot Valve is Open.

Results Entrainment Fraction

Figure 6 shows the mass flow rate removed from the removal slot, which would ideally be the amount of liquid that remained in the liquid film and did not become separated from the wall. As stated previously, figure 5 showed that not all of the liquid was captured by the removal slot in the experiments. Thus, the raw data underpredicts the actual amount of liquid that remained in the liquid film after being injected through the upstream slot. It is very difficult to determine exactly how much liquid skimmed over the slot in all cases from the high speed video images alone. However, the removal flow rate seems to follow a trend in figure 6. Thus, it appears as though the amount of film that ran over the slot in the experiments introduced some sort of bias error to all the conditions studied.

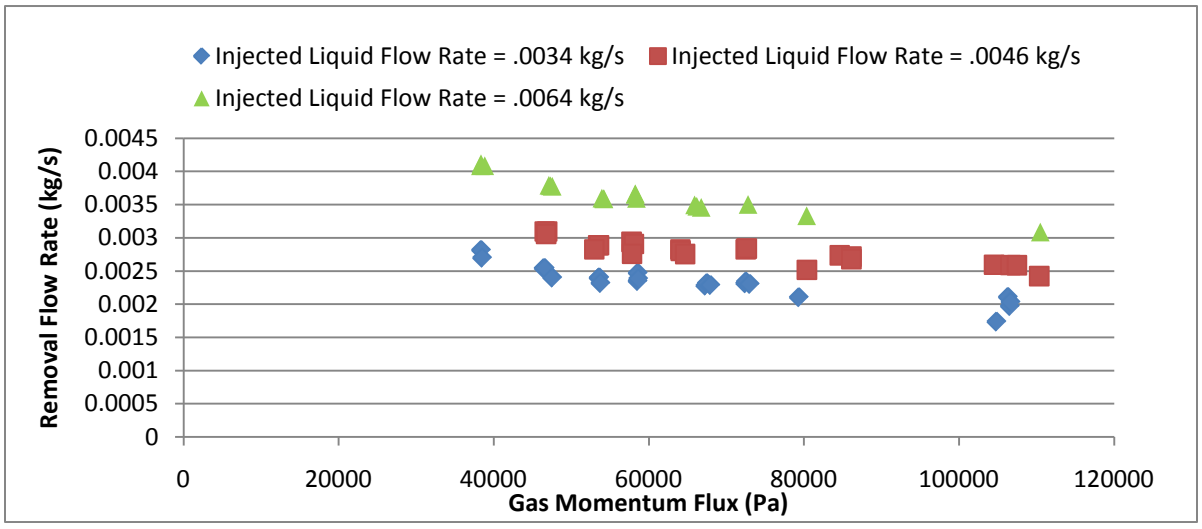

Figure 6: Liquid Film Removal Flow Rate Vs Gas Momentum Flux

Figure 7 shows the fraction of liquid entrained into the gas phase as a function of gas momentum flux for several different injected liquid flow rates. The results are compared with the entrainment fraction proposed by Gater, Ebner, and Sawant. The entrainment fraction in our experiment seems to be much higher than the entrainment fraction predicted by any of the these correlations. Thus, it appears as though at least 10-25% or more of the liquid film may be running over the removal slot, which would cause the entrainment fraction to be overpredicted. Additional descrepancies between the data and the correlations could also be due to the geometry of the injection slot. Gater, Ebner, and Sawant introduced their films either tangentially with the gas or through a large porous medium. However, as shown in figure 4, our films were injected through a thin slot perpendicular to the gas flow. This configuration may have resulted in additional mass loss at the point of injection that is not accounted for the correlations shown in figure 7. Despite these descrepancies, the entrainment fraction observed in our experiment seems to exhibit similar trends to the correlations proposed by Gater and Ebner. Though Gater's correlation does not account for any dependence on the injected liquid flow rate, the slope and curvature of the data exhibited by each of the 3 different liquid flow rates in our experiment seems to follow the general trend of Gater's correlation quite well. Ebner's correltion seems to suggest that the dependence of the entrainment fraction on the liquid flow rate should not be as strong as what is observed in this experiment. Note that the mechanism for removing the liquid film therefore needs to be modified before any definitive conclusions are drawn from this data.

While Sawant's correlation was not intended to be applied to the geometry of our experiment,[11] it is interesting to note that Sawant's correlation predicts that virtually no entrainment should have occurred for liquid flow rates less than about .0064 kg/s. Therefore it is also possible that results from the removal slot may be indicating an entrainment fraction when there should not be one. However, it is not possible to confirm this until the removal slot has been modified.

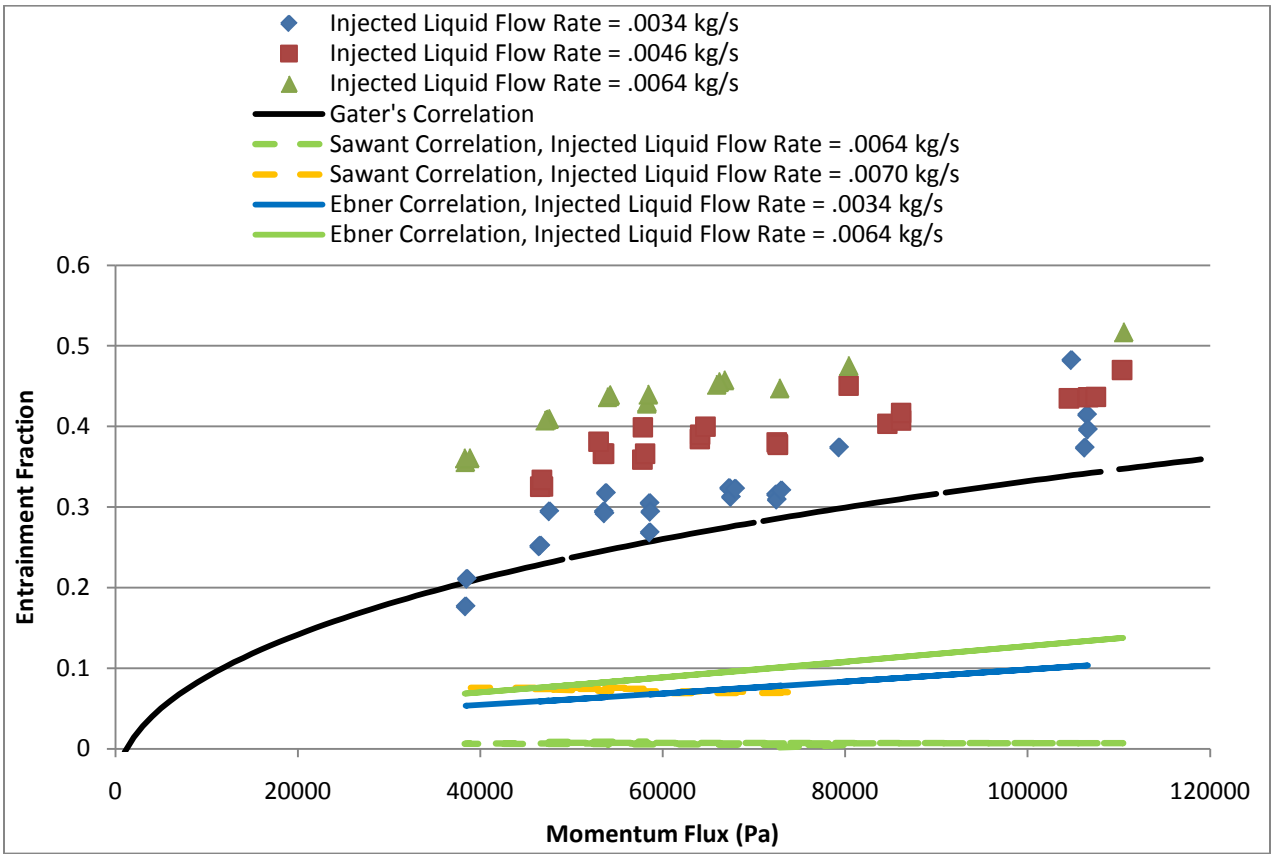

Figure 7: Fraction of Liquid Entrained into Gas Phase Vs Gas Momentum Flux

Results LFD

Figure 10 displays the raw data of relative film position taken by the LFD during a typical test run. In addition to the relative position of a surface, the LFD also records the intensity of the light intensity peak on a scale of 1-255. Different surfaces that fall within the range of the focal point of the LFD usually reflect light intensities of different strengths. Thus, it is possible that the LFD can be used to discriminate between two different surfaces based on the relative strengths of the light intensities corresponding to each surface. This can be very important in deciphering which surface is which in dynamic applications, such as when measuring the thickness of shear-driven film flows. For example, in our application it was observed that the intensity of light reflected to the LFD from the surface of still water did not exceed 70, and that the intensity of the light intensity peaks typically varied between 30-70 when the surface was disturbed. The light intensity peaks reflected from the dry aluminum substrate upon which the film ran were typically about 180. With a turbulent liquid film running over the aluminum surface, the strongest signal reflected back to the LFD was observed to never drop below 135. Based on this knowledge, the strongest light intensity peak received by the LFD during measurements was assumed to correspond with the aluminum surface and the second strongest light intensity was assumed to correspond with the surface of the liquid film.

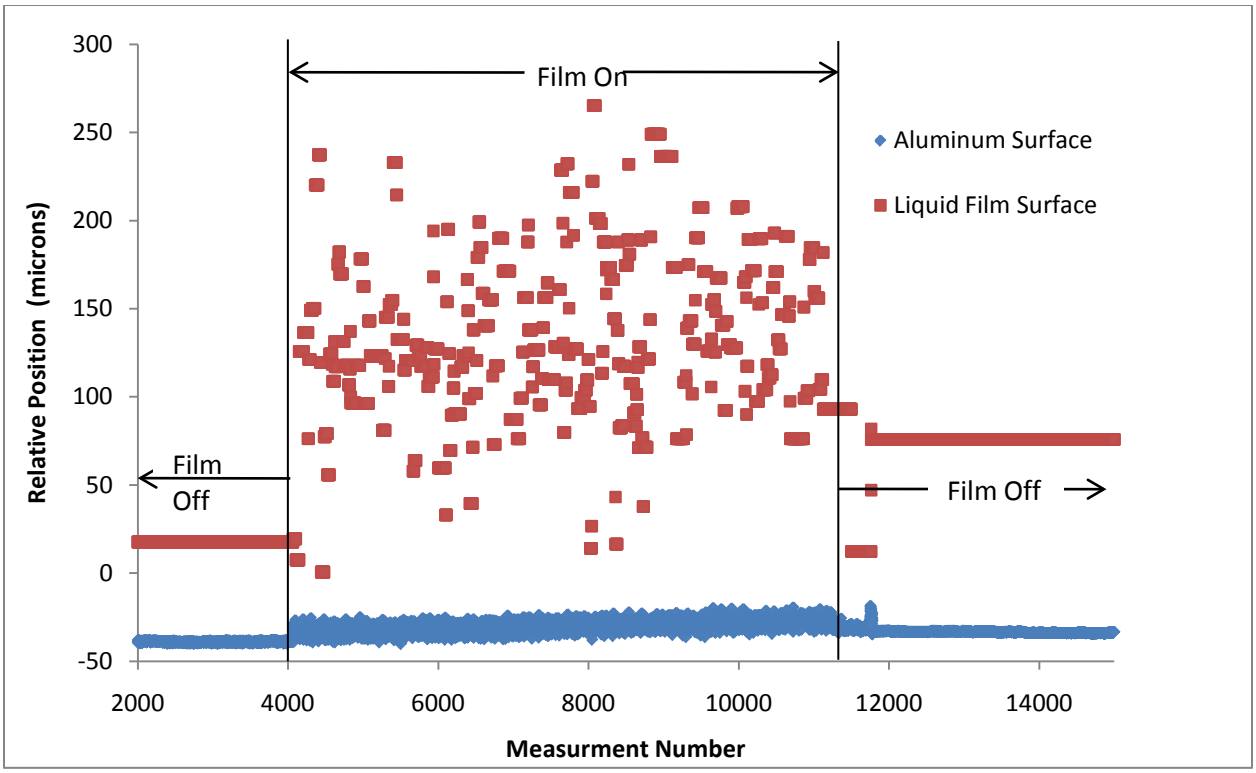

Figure 10: Raw Relative Position Data from the LFD

Much of the data that was believed to correspond with the surface of the liquid film in Figure 10 is repeated several times in a row. This results from the fact that, in the event that LFD is unable to detect a second highest intensity light peak, then the LFD simply outputs the previous measured value. Similarly, in the event that the LFD is unable to detect any light intensity peak, then the previous value for both signals will simply be repeated. Before the film flow is initiated, there is no second highest light intensity to be received by the LFD, as only the aluminum surface is present to reflect a signal. Therefore, the LFD continues to output the last measurable value from what was assumed to be the film surface from the previous run. This explains the straight line from the "Liquid Film Surface" data in figure 10. Once the film is turned on, the "Liquid Film Surface data" becomes very scattered. As demonstrated by Wegener, the LFD is incapable of measuring the surface of the liquid film if the surface angle exceeds 8 degrees. As the film surfaces were highly turbulent in all experiments, it is expected that LFD would not always be able to measure the location of the surface of the liquid film. Thus, much of the "Liquid Film Surface" data is repeated, due to the LFD not receiving a reflection of sufficient intensity.

The intensity of the light reflected from the aluminum surface was not observed to fall below a value of 130 during any of the experiments. Thus, none of the data from the aluminum surface was repeated due to a failure of

the LFD to detect a reflection of sufficient intensity. In addition, when the film is turned on, the surface of the aluminum seems to jump up to a new position. This results from the fact the laser being reflected off of the aluminum surface now has to pass through the liquid film, which shifts the focal point of the LFD due to the film's index of refraction.

Two methods can be used to estimate the thickness of the liquid film. The first method, hereafter referred to as "method 1," involves estimating the thickness of the liquid film by taking the difference the "Liquid Film Surface" data and the position of the aluminum substrate. However, the relative position of the aluminum substrate is unknown when the film is running along the surface because the liquid film interferes with the laser beam. Secondly, the nitrogen air flow is usually colder than ambient, which would cause the entire test article to contract due to temperature changes. This effect generally brings the aluminum surface closer to the LFD. Figure 11 presents a close up view of the signal being returned from the aluminum surface, which shows that the relative position of the aluminum surface is higher after the test run than it is before the test run. To account for this, a linear trend line was applied to the data in order to estimate the relative position of the aluminum surface during a test run. Thus, in method 1, the film thickness can be estimated by finding the difference between "Liquid Film Surface" data and this trend line.

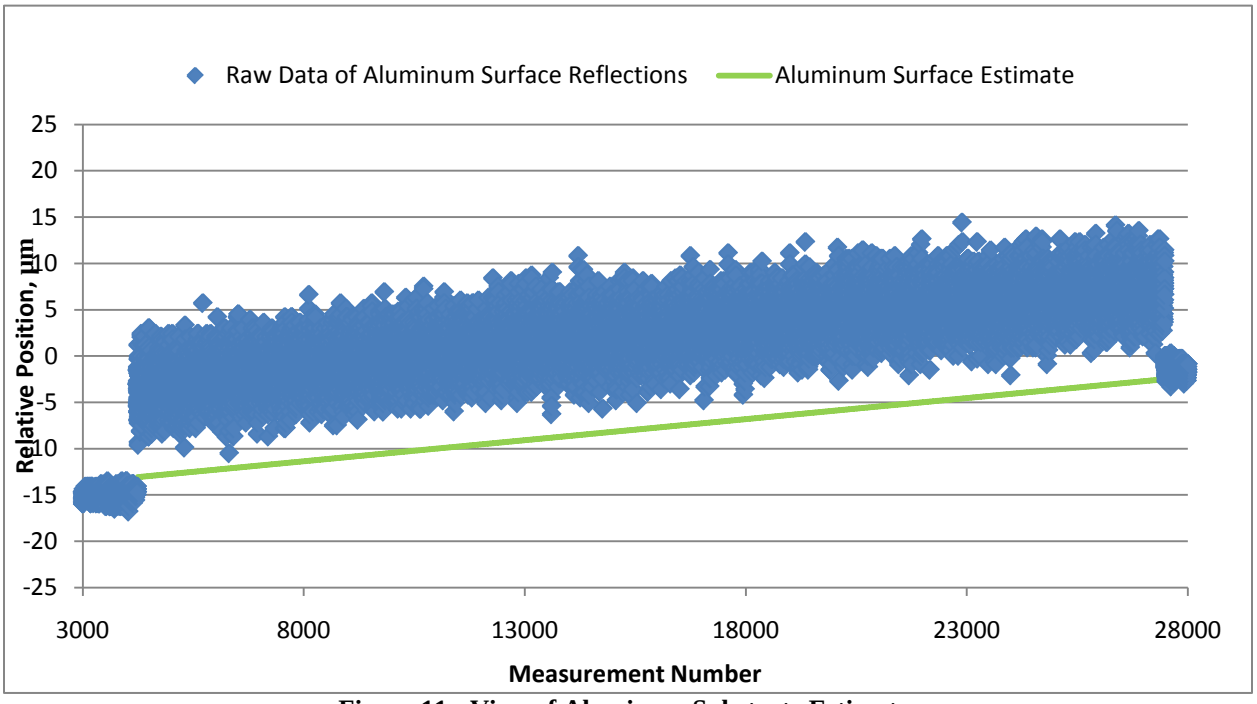

Figure 11: View of Aluminum Substrate Estimate

The thickness of the liquid film can also be estimated from the shift observed in the "Aluminum Surface" data by tracking the path of the beam as it passes through a liquid film. Figure 12 shows an illustration of this problem. The dotted red line in the figure represents where the focal point of the LFD would be in the presence of no film. The solid red line represents the actual beam that is reflecting off of the aluminum surface. The shift observed in the "Aluminum Surface" data, f_{shift}, is equal to $\delta_l - f_l$, or $\delta_r - f_r$. f_{shift} can be estimated throughout the experiment by subtracting the relative position of the trend line represented in figure 11 from the "Aluminum Surface" data.

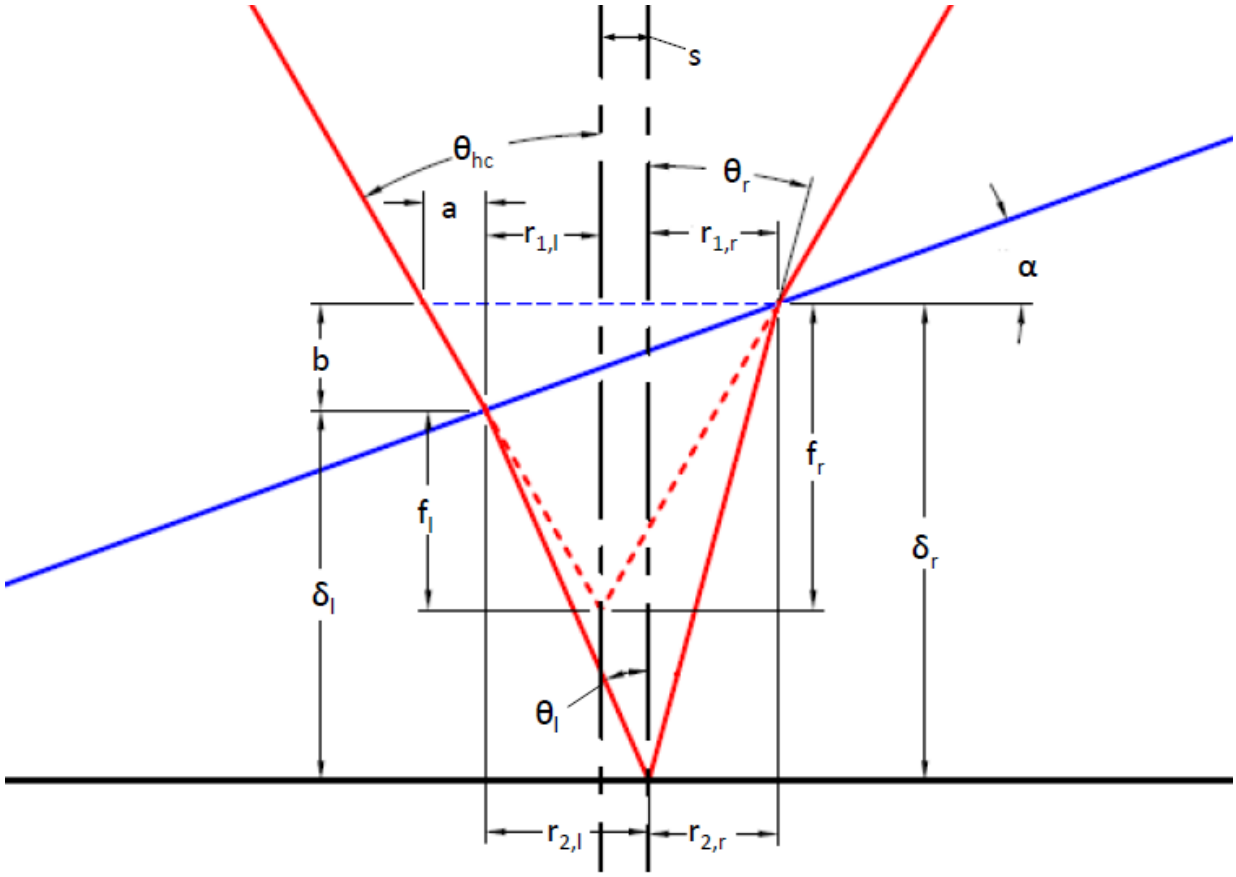

Figure 12: Illustration of the LFD's Conical Laser Beam Passing Through the Surface of The Liquid Film and Reflecting off of the Aluminum Surface.

Assuming that the shift in the focal point and the angle of the film are known, then film thickness on the left of the diagram, denoted δ_l, can be calculated from:

$$f_{shift} = \delta_l \cdot \left(1 - \frac{\tan\theta_l - s'}{\tan\theta_{hc}}\right) \quad (eq.14)$$

where s', θ_r, θ_l, can be calculated from:

$$s' = \frac{1}{2}\left(\tan\theta_l + \left(\left(\frac{1+\tan\alpha\tan\theta_l}{1-\tan\alpha\tan\theta_r}\right) - 1\right) \cdot \tan\theta_{hc} - \left(\frac{1+\tan\alpha\tan\theta_l}{1-\tan\alpha\tan\theta_r}\right) \cdot \tan\theta_r\right) \quad (eq.15)$$

$$\theta_l = \sin^{-1}\left(\frac{n_1}{n_2}\sin(\theta_{hc} - \alpha)\right) + \alpha \quad (eq.16)$$

$$\theta_r = \sin^{-1}\left(\frac{n_1}{n_2}\sin(\theta_{hc} + \alpha)\right) - \alpha \quad (eq.17)$$

With δ_l calculated, δ_r can be determined by:

$$\delta_r = \delta_l \cdot \left(\frac{1+\tan\alpha\tan\theta_l}{1-\tan\alpha\tan\theta_r}\right) \quad (eq.18)$$

Then, the average film thickness for the given angle and shift in the focal point can be found with:

$$\delta_{ave} = \frac{f_{shift}}{2\left(1 - \frac{\tan\theta_l - s'}{\tan\theta_{hc}}\right)}\left(1 + \frac{1 + \tan\alpha\tan\theta_l}{1 - \tan\alpha\tan\theta_r}\right) \quad (eq.\,19)$$

This method for estimating the film thickness is herein referred to as "method 2."

The actual film thickness compared to f_{shift} is dependent on the surface angle of the liquid film. Figure 13 represents δ_{ave}/f_{shift} as a function of the angle of the liquid film surface. This figure demonstrates that the apparent shift in the focal point of the LFD is a strong function of the surface angle of the liquid film, and, therefore, in order for "method 2" to give an accurate estimate of the average film thickness, an estimate of the surface angle on the liquid film must be known. In addition, in reality, the film surface will have some curvature to it; this could also shift the focal point due to a lensing effect. Finally, the above analysis is based only on geometric optics. The effects of the wave nature of light are not accounted for.

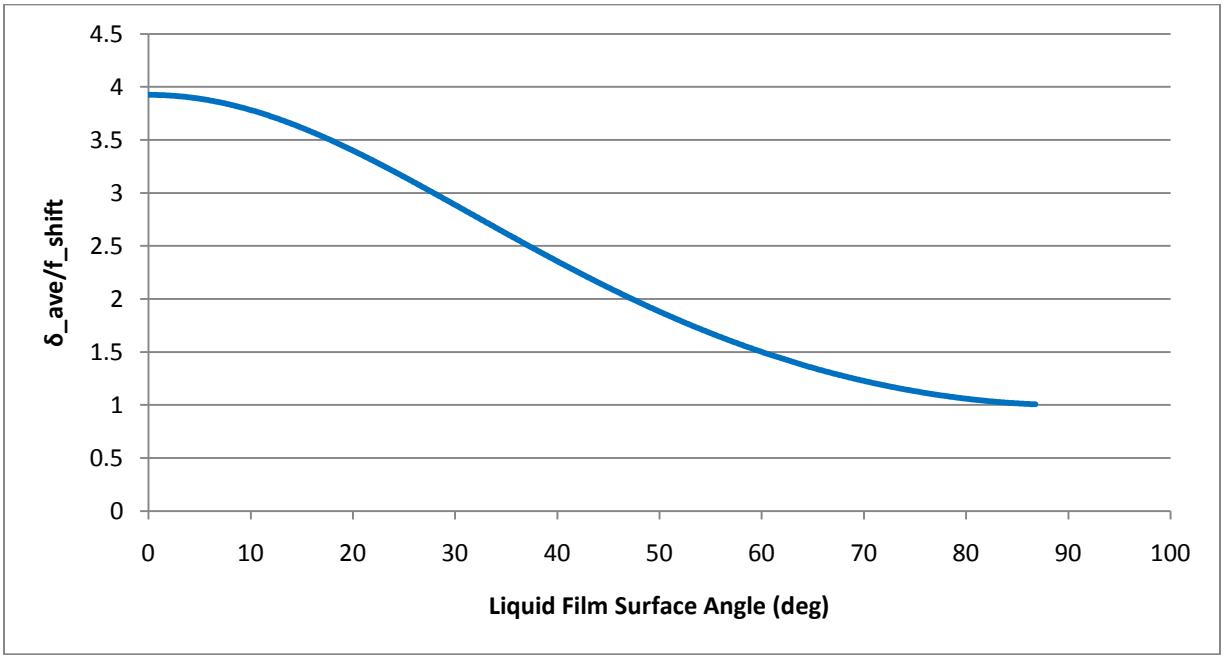

Figure 13: Plot Showing how the Liquid Film Surface Angle Shifts the Focal Point of the LFD

Assuming that the most of the surface angles on the film never exceed 8 degrees, an estimate of the film thickness using "method 2" was obtained. Thus, a $\delta_{ave}/f_{shift} = 3.9$ was assumed in estimating the film thickness using method 2. Note that this would place a maximum estimate on the film thickness using for "method 2."

Figures 14 though 16 show histogram plots of the film thickness estimates for several test conditions using each method. The plots are not normalized. For the film thickness estimates determined using "Method 1," the repeated data points are removed for the generation of the histogram. The histogram plots determined using each method resemble a normal distribution. Thus, an estimate of the average film thickness for a test condition can be obtained from the peak of each histogram.

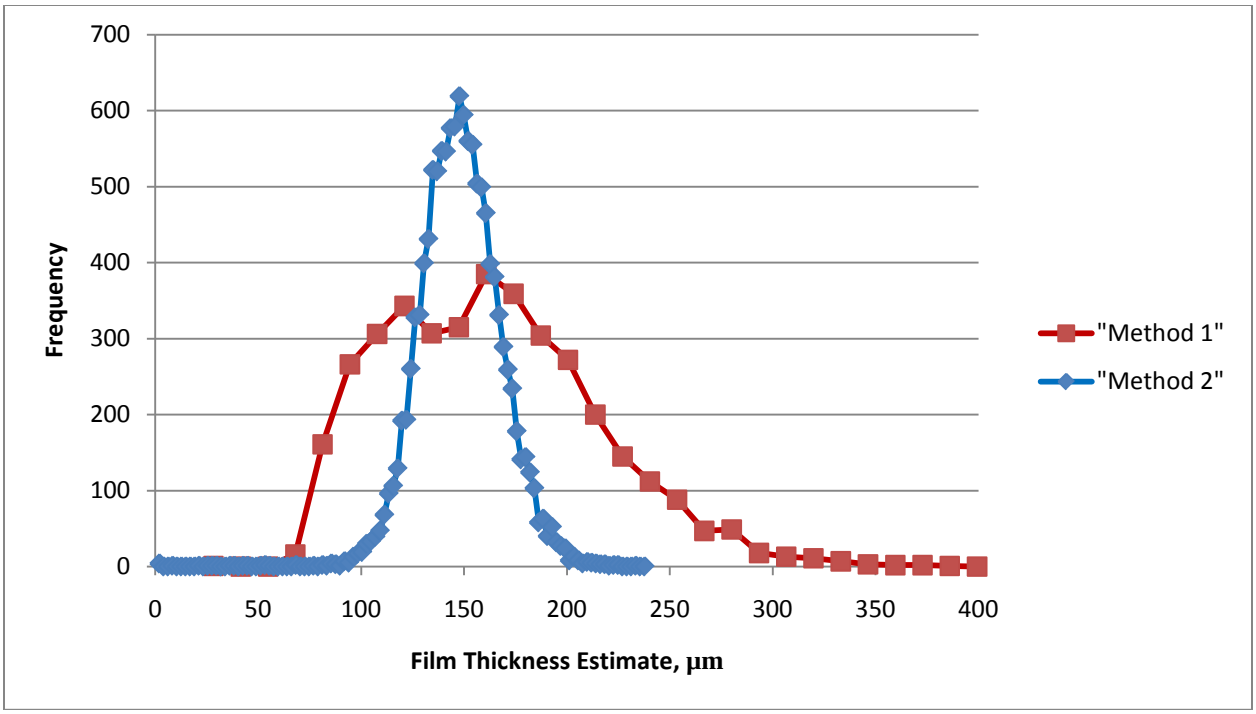

Figure 14: Histogram of Film Thickness Estimates for Each Method with Momentum Flux = 2,970 Pa and Liquid Film flow rate = .007 kg/s

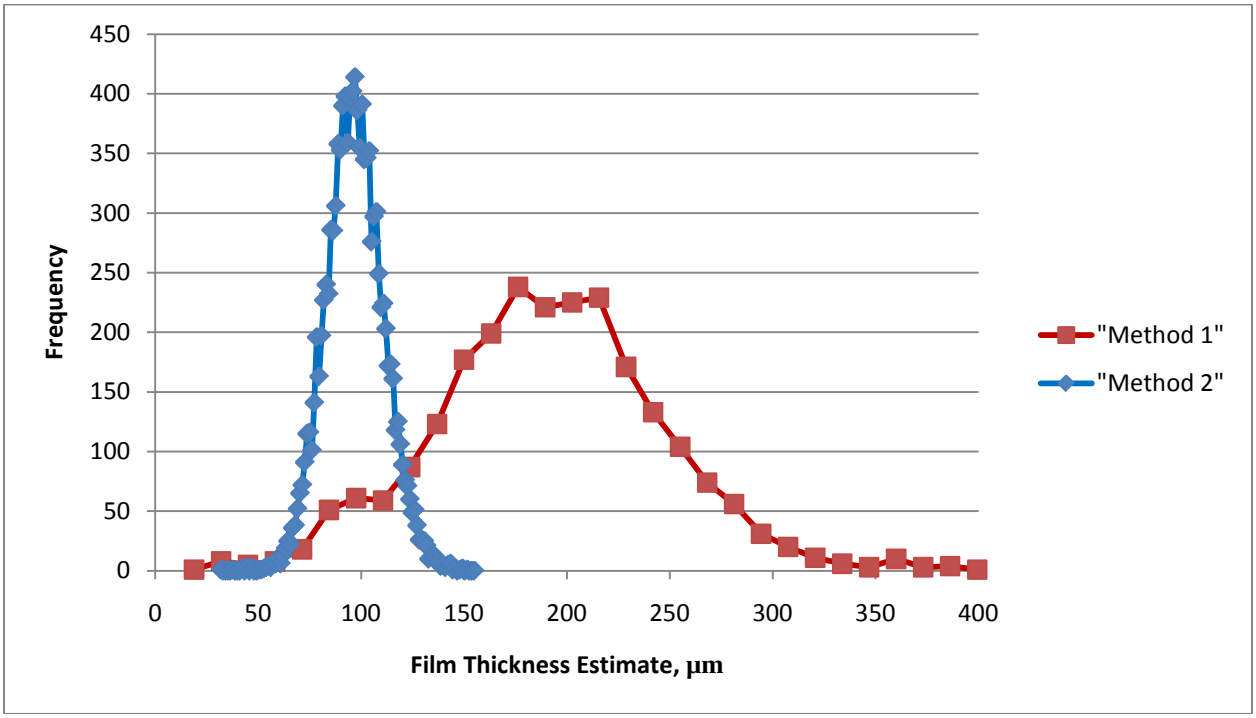

Figure 15: Histogram of Film Thickness Estimates for Each Method with Momentum Flux = 7,750 Pa and Liquid Film flow rate = .007 kg/s

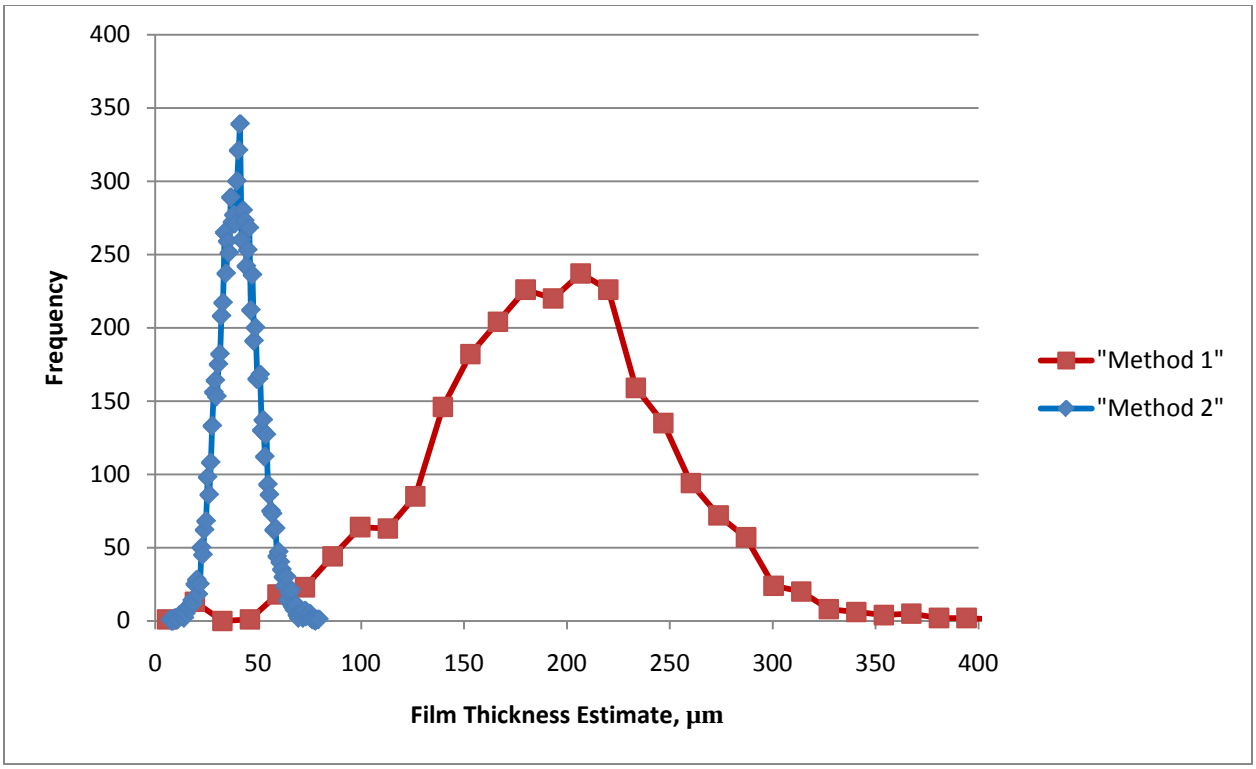

Figure 16: Histogram of Film Thickness Estimates for Each Method with Momentum Flux = 38,300 Pa and Liquid Film flow rate = .007 kg/s

Figure 14 shows that the average film thickness estimated from both methods are generally in very good agreement with each other at very low momentum fluxes, when the amount of liquid entrained is low. The peaks of the histograms for each method correspond very well with each other. However, method 2 is not able to account for the wide variations in film thickness that "method 1" was able to resolve. This is expected because in order for "method 2" to account for all the variations in film thickness, all the variations in surface angle in curvature would need to be accounted for when calculating δ_{ave}/f_{shift}. Yet, the average film thickness estimates obtained using both methods do agree very well with each other at low momentum fluxes. Therefore, it does appear as though "method 2" gives a valid approximation of the average film thickness for a test run, at least when momentum fluxes are low.

Figures 15 and 16 show that the film thickness estimates for each method begin to deviate substantially from each other once the momentum flux of the gas, and therefore the entrained fraction increases. The estimate of the average film thickness using "method 1" increases when the momentum flux is increased from 2,970 Pa in figure 14 to 7,750 Pa in figure 15. Then, there doesn't seem to be a significant change in the histograms between figures 15 and 16, yet the momentum flux is nearly tripled. On the other hand, the average film thickness predicted by method 2 is seen to decrease with increasing momentum flux as one would expect. Thus, it appears as though "method 2" might be a more valid way to estimate the film thickness when the LFD is orientated such that the laser passes through the film before reflecting off the substrate.

From analysis of the LFD data, it appears as though the "Liquid Film Surface" data shown in figure 10, do not actually correspond with the surface of the liquid film in most of the experiments as was assumed. Rather, it is speculated that the droplets that are stripped off the film seem to be forming a droplet heavy layer just above the film that seem to be scattering more light back to the LFD than what is being reflected off of the liquid film surface. Therefore, orientating the LFD such that it measures the thickness of the liquid film by passing the laser beam through a transparent substrate, as shown in the left hand side of Figure 3, might be a better way to measure film thickness. This would avoid the issue of entrained droplets interfering with the laser beam.

Future Work

As stated previously, several improvements need to be made to the test article and diagnostics before any definitive quantative conclusions can be made. First, the film removal slot needs to be adjusted or remade such that

it captures most of the film. Second, the film injection slot should be made a couple hundredths of an inch wider so that the film spans the test article. Lastly, additional work needs to be done in order to qualify the LFD's applicabiltiy to measuring liquid film thicknesses driven by high-momentum flux gas flows.

Once improvements to the test article have been made and after the LFD has been qualified, experiments at both lower and higher momentum fluxes with water should be run. Fluids with various surface tensions and viscosities should also be run to better reduce Weber and Reynolds number importance on the entrainment fraction of the liquid phase. Eventually, experiments at momentum fluxes of over 1,000,000 Pa should be conducted in order to determine film behavior at momentum fluxes characteristic of high pressure, high performance liquid rocket engines.

Summary and Conclusions

The literature regarding entrainment from liquid films relevant to rocket conditions is very limited. Several correlations have been proposed, yet many of these correlations seem to be limited to a relatively narrow range of gas momentum fluxes. All experimental research done on shear-driven liquid films have been limited to gas phase momentum fluxes that are about an order of magnitude less than the momentum fluxes encountered in liquid rocket engines. From analysis of the literature, it appears as though the behavior of a shear-driven liquid film and mass transfer due to droplet entrainment is more strongly dependent on surface tenstion and gas momentum flux at low gas momentum fluxes. However, at higher gas momentum fluxes, the behavior of the films appears to change, and then the entrainment seems to also be dependent on viscosity and liquid film flow rate, and less dependent on surface tension.

A test apparatus was constructed at AFRL to investigate the establishment of a liquid film from a slot injector under a range of gas momentum fluxes and liquid flow rates. Data on the film thickness and entrainment fraction were obtained. Problems with the experiment have prevented any definitive conclusions from being drawn as of yet. Nonetheless, the trends seen in the entrainment fraction data thus far seem to generally follow some of the trends predicted by correlations in the literature.

The film thickness data that has been acquired with the LFD still needs to be qualified. The two methods that were used for determining the thickness of the liquid film do not correspond with each other. A possible reason for this discrepancy is that the droplets entrained from the liquid film and the highly turbulent surface of the liquid film may be interfering with one or both of the signals being returned to the LFD. At this time, the liquid film thickness obtained by correcting for the shift in the focal point as the LFD laser passes through the liquid film and reflects off the aluminum substrate agrees with the film thickness estimates of Coy better than the other method. Additional studies still need to be performed on the LFD in order to qualify its ability to measure film thicknesses in the conditions of this experiment.

Acknowledgements

The authors would like to thank Alex Schumaker, Steve Dancyk, Malissa Lightfoot, Dave Hill, John Haiser, and Edgar Felix at AFRL/RZSA for contributions to the experiment. The authors would also like to thank Jeff Wegener at AFRL/RZSA and UCLA for his insights on the operation and use of the LFD.

Ryan Miller would like to give special thanks his advisor, Dr. Anderson at Purdue University, and to AFRL/RZSA for granting him the opportunity to work on this project.

References

[1]Volkman, J. C., Tuegel, L. M., McLeod, J. M., "Gas Side Heat Flux and Film Coolant Investigation for Advanced LOX/Hydrocarbon Thrust Chambers," *AIAA/SAE/ASME/ASEE 26th Joint Propulsion Conference*, American Institute of Aeronautics and Astronautics, Orlando, FL, July 16-18, 1990, AIAA 90-2184

[2]Kirchberger, C., Schlieben, G., Hupfer, A., Kau, H., Martin, P., Soller, S., "Investigation on Film Cooling in a Kerosene/GOX Combustion Chamber," *45th AIAA/ASME/SAE/ASEE Joint Propulsion Conference and Exhibit*," American Institute of Aeronautics and Astronautics, Denver, CO, Aug. 2009, AIAA 2009-4824.

[3]Wegener, J. L., Drallmeier, J. A., "Measurement of Thin Liquid Film Characteristics using Laser Focus Displacement Instruments for Atomization Applications," *ILASS-Americas 22nd Annual Conference on Liquid Atomization and Spray Systems*," Cincinnati, OH, May 2010.

[4]Hazuku, T., Fukamachi, N., Takamasa, T., Hibiki, T., Ishii, M., "Measurement of Liquid Film in microchannels using a laser focus displacement meter," *Experiments in Fluids*, Vol. 38, No. 6, 2005, pp. 780-788

[5]Yu, Y. C., Schuff, R. Z., Anderson, W. E, "Liquid Film Cooling Using Swirl in Rocket Combustors," *40th AIAA/ASME/SAE/ASEE Joint Propulsion Conference and Exhibit*, American Institute of Aeronautics and Astronautics, July 2004, AIAA 2004-3360
[6]Kinney, G. R., Abramson, A., E., Sloop, J. L. "Internal Liquid Film Cooling Experiments with Air-Stream Temperature to 2000ºF in 2- and 4-Inch Diameter Horizontal Tubes," NACA Report 1087, 1952
[7]Knuth, E. L., "The Mechanics of Film Cooling- Part 1," *Jet Propulsion*, Vol. 24, No. 6, 1954, pp. 359-365.
[8]Coy, E. B., Schumaker, S. A., Lightfoot, M. A., "Film Cooling of Liquid Hydrocarbon Engines for Operationally-Responsive Space Access," *JANNAF 5th Liquid Propulsion Subcommittee Meeting*, Colorado Springs, CO, May 2009.
[9]Gater, R., A., L'Ecuyer, M. R., "A Fundamental Investigation of the Phenomena that Characterize Liquid Film Cooling," Jet Propulsion Center, TM-69-1, Jan. 1969.
[10]Ebner, J., Gerendás, M., Schäfer, O., Wittig, S., "Droplet Entrainment From a Shear-Driven Liquid Wall Film in Inclined Ducts: Experimental Study and Correlation Comparison," *Journal of Engineering for Gas Turbines and Power*, Vol. 124, No. 4, Oct. 2002, pp. 874-880.
[11]Sawant, P., Ishii, M., Mori, M., "Predition of amount of entrained droplets in vertical annular two-phase flow," *International Journal of Heat and Fluid Flow*, Vol. 30, No. 4, Aug. 2009, pp. 715-728